Applied Catalysis B: Environmental 154–155 (2014) 44–50

Contents lists available at ScienceDirect

Applied Catalysis B: Environmental

journal homepage: www.elsevier.com/locate/apcatb

Characterization and photostability of Cu_2O–Ag–AgBr/Al_2O_3 for the degradation of toxic pollutants with visible-light irradiation

Xuexiang Hu, Xuefeng Zhou, Ran Wang, Chun Hu*, Jiuhui Qu

State Key Laboratory of Environmental Aquatic Chemistry, Research Center for Eco-Environmental Sciences, Chinese Academy of Sciences, Beijing 100085, People's Republic of China

ARTICLE INFO

Article history:
Received 27 November 2013
Received in revised form 28 January 2014
Accepted 4 February 2014
Available online 13 February 2014

Keywords:
Ion release
Plasmonic photocatalyst
Visible light irradiation
Nanocomposites
Toxic organic pollutant

ABSTRACT

A plasmonic photocatalyst Cu_2O–Ag–AgBr supported on mesoporous alumina (Cu_2O–Ag–AgBr/Al_2O_3) was prepared by deposition–precipitation methods. The samples were characterized by means of X-ray diffraction (XRD), transmission electron microscopy (TEM) and X-ray photoelectron spectroscopy (XPS). The results indicated that Cu_2O–Ag–AgBr nanojunctions were formed by the contact of Cu_2O, AgBr and Ag with each other. The catalyst showed high photocatalytic activity and stability for the degradation of toxic persistent organic pollutants under visible light irradiation. The release of metal ions from the catalyst was significantly inhibited during the photodegradation of pollutants. Four interfacial electron transfer process were verified in the photoreaction system of Cu_2O–Ag–AgBr/Al_2O_3 on the basis of electron spin resonance and cyclic voltammetry analyses under a variety of experimental conditions. The results indicated that the coupling of Cu_2O with Ag NPs and AgBr not only accelerated interfacial electron transfer processes, leading to the fast photoreduction of the dissolved Ag^+ and the photostability of Cu_2O. These findings could be useful for the practical application of plasmonic visible light photocatalyst and photovoltaic fuel cells.

1. Introduction

Semiconductor–metal nanocomposites have been widely employed in photocatalysis and considered as a promising alternative to solve many environmental and energy issues [1–4]. In particularly, nanoparticles (NPs) of noble metals can strongly absorb visible light because of surface plasmon resonance, which greatly enhances the overall photocatalytic efficiency at the interface between the metal and the semiconductor [5–11]. Many plasmonic photocatalysts have been developed based on this phenomenon using a combination of Ag or Au NPs and semiconductor [3,11–15]. The electron transfer was based on both photoexcitation of semiconductor and plasmon-excitations of noble metal NPs on the surface [14,16,17]. The electron injection from surface plasmon resonant noble metal NPs into semiconductor and resultant oxidation of the noble metal NPs to ions, which is released into the aqueous, has been evidenced previously [18–20]. Therefore, the corrosion and dissolution of the noble metal NPs is inevitable in the photocatalytic reaction, limiting the practical application of plasmonic photocatatlysts [16,21].

It is possible that enhancing electron transfer may not only inhibit metal ion release, but also improve photocatalytic efficiency [22]. One factor that potentially influences the electronic properties of the nanocomposite is the size of the noble metal particles. For example, previous study has demonstrated the influence of gold NPs deposition on the overall energy and catalytic activity of TiO_2 [2]. In addition, the different surface potential in multimetal assemblies or metal–semiconductor heterojunction may also influence interfacial electron behavior [23]. Our previous study demonstrated that the coupled Au and Ag NPs exhibited high photosensitivity and photostability in Au–Ag–AgI/Al_2O_3 [22]. Besides, it is known that the composite of two semiconductive oxides may enhance the opto-electrical properties due to the difference in band gap structures. The matching band potentials facilitated the fast transfer and separation of the photoinduced carriers [1]. p-type cuprous oxide (Cu_2O) not only make good use of visible light as photocatalyst directly, but also can be used as sensitized semiconductor for a solar cell. Cu_2O with a CB level of −1.4 eV-SHE, is known to be one of the oxides with high level of conduction bands [24]. Therefore, the photogenerated electrons in Cu_2O can easily transfer to other semiconductor [25] or be captured by O_2 and H_2O [26]. It is expected that the electron transfer of plasmonic photocatalysts can be further improved by the effective modification of Cu_2O.

Recently, we reported that Ag–AgBr/Al_2O_3 exhibited high photocatalytic activity for the degradation and mineralization of

* Corresponding author. Tel.: +86 10 62849171; fax: +86 10 62923541.
E-mail address: huchun@mail.rcees.ac.cn (C. Hu).

http://dx.doi.org/10.1016/j.apcatb.2014.02.003
0926-3373/

pollutants, due to the Ag NPs plasmon-assisted effect on the AgBr photocatalyst [27]. However, the electron injection from Ag NPs to AgBr, resulted in the oxidation of some Ag NPs to Ag^+, which were dissolved in water and resulting in secondary water pollution [18]. In this paper, Cu_2O–Ag–AgBr/Al_2O_3 composites were prepared by deposition–precipitation. Cu_2O–Ag–AgBr/Al_2O_3 exhibited efficient photocatalytic activity under visible light irradiation and the release of Ag^+ was successfully inhibited to low levels. A plasmon-mediated photocatalytic mechanism was verified by electron spin resonance (ESR) and cyclic voltammetry (CV) analyses under a variety of experimental conditions. A metal ion-releasing suppression mechanism was proposed.

2. Experimental

2.1. Chemicals and materials

The reagent poly(ethylene glycol)-block-poly(ethylene glycol) (P123), was purchased from Sigma Chemical Co. 5-Tert-butoxycarbonyl 5-methyl-1-pyrroline N-oxide (BMPO) was purchased from the Bioanalytical Lab (Sarasota, FL). All other chemicals used were analytical grade, purchased from Beijing Chemical Co. and used without further purification.

2.2. Preparation of catalysts

Mesoporous γ-Al_2O_3 was prepared from precursors of aluminum *i*-propoxide in the presence of glucose in aqueous system as described previously [28]. Cu_2O nanocubes were prepared as described previously, and stored in refrigerator before used [29]. Then, Cu_2O was deposited onto Al_2O_3 during the deposition–precipitation process of Ag–AgBr as reported in our previous work [27]. Briefly, 0.08 g of Cu_2O and 0.6 g of γ-Al_2O_3 was added to 60 mL of distilled water, and the suspension was sonicated for 30 min. Then 0.13 g of KBr was added to the suspension, and the mixture was stirred magnetically for 30 min, and then sonicated for 30 min. Subsequently, 0.6 g P123 was added to the suspension, and the mixture was stirred magnetically 30 min and then sonicated for 30 min. Then, 0.13 g of $AgNO_3$ in 1.8 mL of $NH_3.H_2O$ (25 wt% NH_3) was quickly added to the mixture. The resulting suspensions were stirred at room temperature for 12 h. All the above processes were carried out in a dark situation. Then, the amount of Ag and Cu ions in the supernatant was measured by inductively coupled plasma-optical-emission spectrometry (ICP-OES) on an OPTIMA 2000 (Perkin-Elmer) instrument, confirming that the Ag content of 10 wt% was incorporated in Al_2O_3. And there was not any copper was detected, confirming all the dosage of Cu_2O was deposited. So, the molar ratio of Cu_2O:Ag–AgBr:Al_2O_3 is 1:1:10.59 in Cu_2O–Ag–AgBr/Al_2O_3. The product was filtered, washed with water, and dried at 70 °C. Finally, the powder was calcined in air at 500 °C for 3 h.

2.3. Characterization

The samples were examined by obtaining XRD patterns (XDS-2000 diffractometer; Scintag, Inc., Sunnyvale, CA) and UV–vis diffuse reflectance spectra (Hitachi UV-3100). The high-resolution transmission electron microscopy (HRTEM) images were obtained by using a JEOL-2010 TEM with an acceleration voltage of 200 kV. X-ray photoelectron spectroscopy (XPS) and Auger electron spectroscopy (AES) data were taken on an AXIS-Ultra instrument from Kratos using monochromatic Al Kα radiation and low-energy electron-flooding for charge compensation. All binding energies were calibrated by the C 1s hydrocarbon peak at 284.80 eV. ESR spectra were obtained using a Bruker model A300-10/12 electron paramagnetic resonance spectrometer. The photocurrent from the various samples was measured in a basic electrochemical system (AMETEK Princeton Applied Research, Oak Ridge, TN) with a two-compartment, three-electrode electrochemical cell equipped with

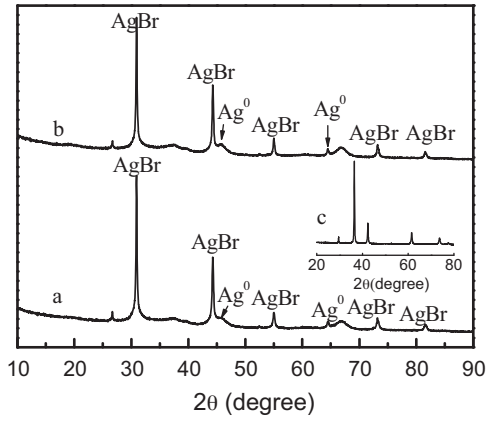

Fig. 1. XRD patterns of (a) Ag–AgBr/Al_2O_3, (b) Cu_2O–Ag–AgBr/Al_2O_3, (c) Cu_2O.

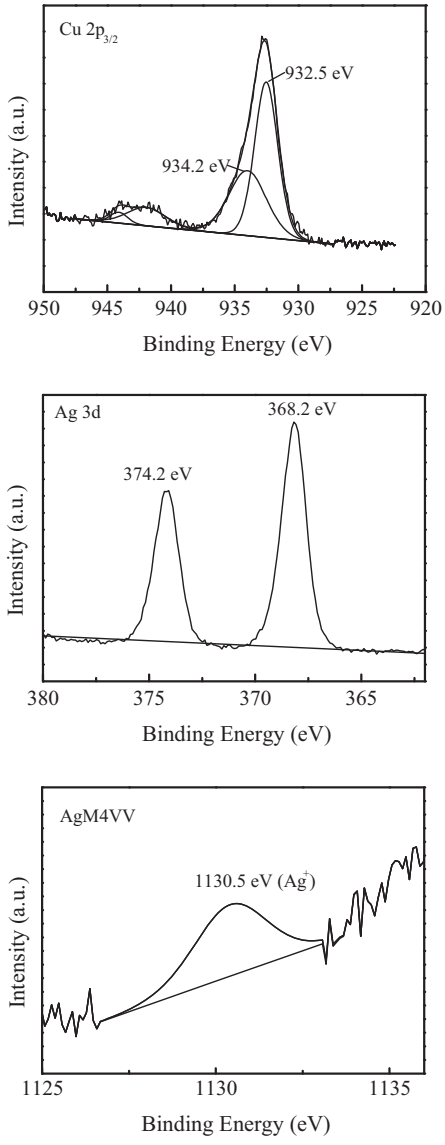

Fig. 2. Cu 2p XPS, Ag 3d XPS and Ag AES spectra for the as prepared Cu_2O–Ag–AgBr/Al_2O_3 sample.

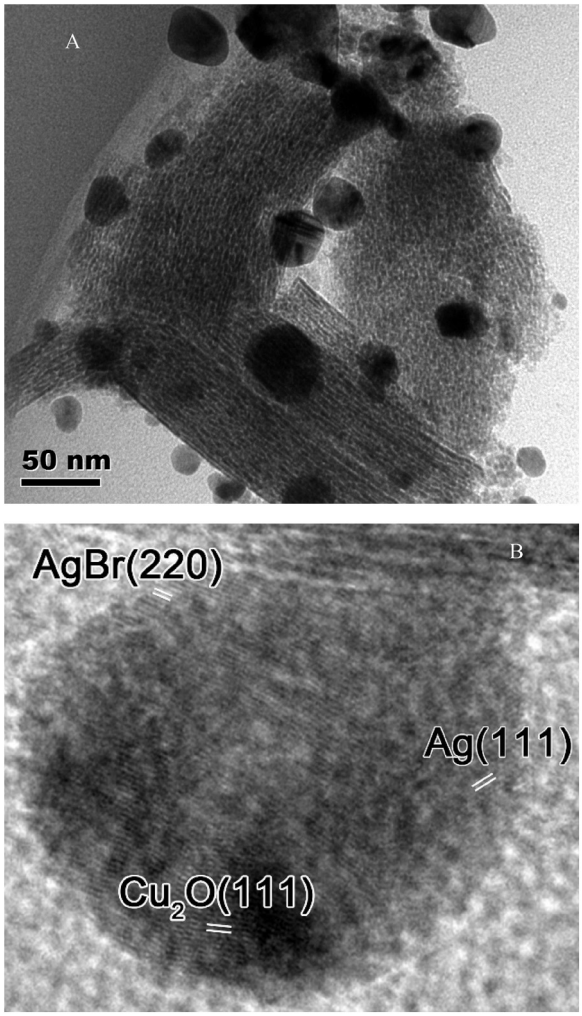

Fig. 3. HRTEM images of Cu_2O–Ag–AgBr/Al_2O_3.

a photocatalyst photoanode (prepared by dip-coating and drying in air at 70 °C) and a platinum wire cathode in a 0.1 M Na_2SO_4 solution. The reference electrode was a saturated calomel electrode.

2.4. Photocatalytic reaction

Photocatalytic experiments were performed in a beaker with aqueous suspensions of 2-chlorophenol (2-CP, 60 mL, 10 mg L^{-1}) and 100 mg of catalyst powder. The 350 W Xe-arc lamp light source, equipped with wavelength cutoff filters for $\lambda > 420$ nm, was focused onto the beaker. The average light intensity was 2.3 mW/cm^2. Prior to irradiation, the suspensions were magnetically stirred in the dark for 30 min to establish adsorption–desorption equilibrium between the pollutants and the surface of the catalyst under room air-equilibrated conditions. The concentration of 2-CP was measured using high-performance liquid chromatography (1200 series; Agilent) with an eclipse XDB-C18 column (5 μm, 4.6 mm × 150 mm; Agilent). The concentration of Ag^+ and Cu^{2+} dissolved in the photoreaction was measured by ICP-OES.

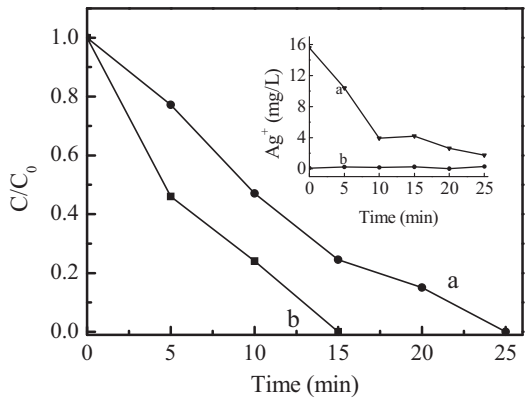

Fig. 5. The photodegradation of 2-CP in aqueous dispersions under visible light irradiation: (a) Ag–AgBr/Al_2O_3, (b) Cu_2O–Ag–AgBr/Al_2O_3. The inset shows the corresponding release of Ag^+.

3. Results and discussion

3.1. Characterization of photocatalysts

Fig. 1 showed the XRD patterns of different samples. The coexistence of Ag (JCPDS 65-2871) and AgBr (JCPDS 06-0438) was observed in both Ag–AgBr/Al_2O_3 and Cu_2O–Ag–AgBr/Al_2O_3. No XRD diffraction peaks of copper oxide species were observed in Cu_2O–Ag–AgBr/Al_2O_3, while the as-prepared Cu_2O was cubic phase (JCPDS 65-3288). This presumably contributed to the incorporation of small particle size and fine dispersion on the surface of Al_2O_3. To affirm the state of the silver and copper on the surface of the Cu_2O–Ag–AgBr/Al_2O_3, the sample was further characterized by XPS and AES measurements. As shown in Fig. 2, the Cu $2p_{3/2}$ spectra can be fitted into two peaks with binding energies at 932.5 eV and 934.2 eV, corresponding to Cu^+ and Cu^{2+}. The additional shake-up satellite peak around 943.2 eV implied the presence

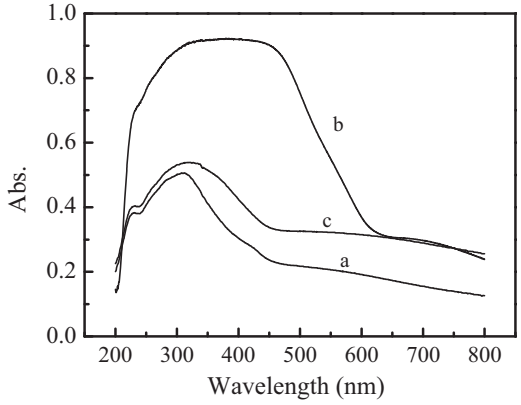

Fig. 4. UV-vis diffuse reflectance spectra of (a) Cu_2O, (b) Ag–AgBr/Al_2O_3, and (c) Cu_2O–Ag–AgBr/Al_2O_3.

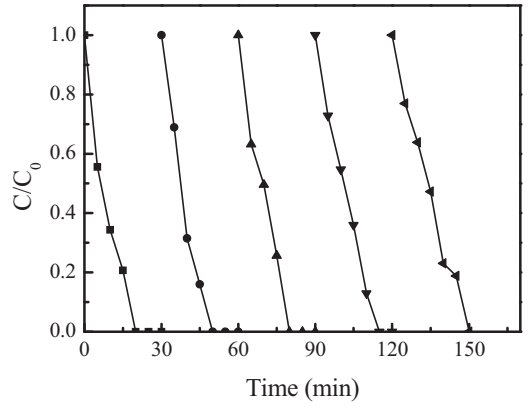

Fig. 6. Cycling runs in the photodegradation of 2-CP in reactivated Cu_2O–Ag–AgBr/MA aqueous dispersion under visible light irradiation.

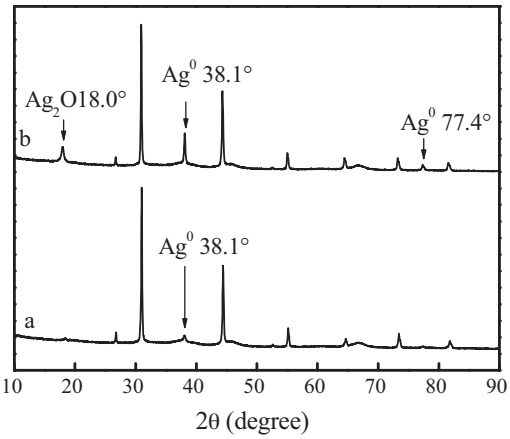

Fig. 7. XRD patterns of Cu_2O–Ag–AgBr/Al_2O_3 after photodegradation of 2-CP under visible light irradiation for (a) 30 min, (b) 40 h.

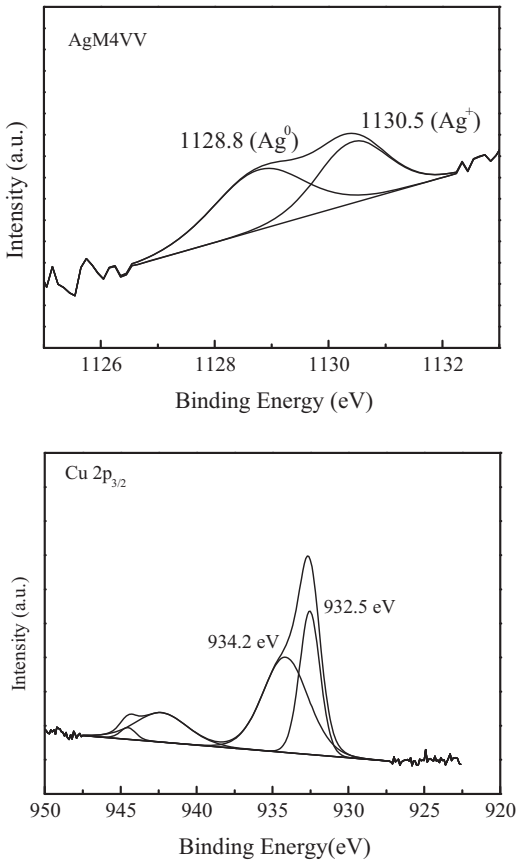

Fig. 8. Ag AES and Cu 2p XPS spectra for the Cu_2O–Ag–AgBr/Al_2O_3 sample after 30 min visible light irradiation in 2-CP solution.

of an unfilled Cu $3d^9$ shell and thus further confirming the existence of Cu^{2+} on the sample surface. The above results confirmed that both Cu^+ and Cu^{2+} exist on the surface, indicating that Cu_2O was oxidized partially to create CuO. According to the peak separation results, the atomic percentage of Cu^+ in mixture of surface Cu^+ and Cu^{2+} is 52%. Fig. 2 also presents the Ag 3d spectra. Peaks around 368.2 eV and 374.2 eV are ascribed to the Ag $3d_{5/2}$ and Ag $3d_{3/2}$ binding energies, respectively. It was very difficult to discriminate the peak position of Ag $3d_{5/2}$ for Ag^+ (368.4 eV) and Ag^0 (368.2 eV) [30]. On the basis of the calculation of the Auger parameter (=BE ($Ag3d_{5/2}$) – Auger (M4VV) + 1486.71 (characteristic energy, eV)) [31], the Auger parameters of Ag was 724.4 eV assigned to Ag^+, indicating that the surface Ag species mainly existed as Ag^+ in as-prepared Cu_2O–Ag–AgBr/Al_2O_3 sample. The Ag^0 species could not be definitely confirmed by XPS and AES measurements due to the lower content. However, the concentration of the surface silver and bromide was 1.16 atom% and 0.63 atom%. The atomic ratio of silver and bromide was about 1.84 more than the stoichiometric ratio of AgBr, indicating the existence of Ag^0 species.

Furthermore, TEM images of Cu_2O–Ag–AgBr/Al_2O_3 shows that Cu_2O, Ag and AgBr nanocomposites were uniformly highly dispersed on the surface of Al_2O_3 (Fig. 3). Their crystalline sizes were in the range 10–20 nm, and the shape was a regular cubic structure. According to the measurement of lattice fringes, d = 0.245 nm, 0.234 nm and 0.204 nm match with the crystallographic planes of Cu_2O (1 1 1), Ag (1 1 1) and AgBr (2 2 0), respectively. This result indicated that Cu_2O, AgBr and Ag were effectively interfaced with each other. The formation of Cu_2O–Ag–AgBr nanojunctions could be favorable for interfacial charge transfer among the three components, enhancing photocatalytic activities of the composites. The diffuse reflectance UV–vis spectra of Cu_2O, Cu_2O–Ag–AgBr/Al_2O_3 and Ag–AgBr/Al_2O_3 were compared in Fig. 4. Cu_2O nanoparticles had a broad adsorption peak at about 600 nm. Ag–AgBr/Al_2O_3 exhibited a visible absorption band around 400–700 nm. The peak around 410 nm could be attributed to the plasmon resonance of Ag NPs. Cu_2O–Ag–AgBr/Al_2O_3 had a much stronger UV and visible absorption than Ag–AgBr/Al_2O_3 due to the mixed absorption of

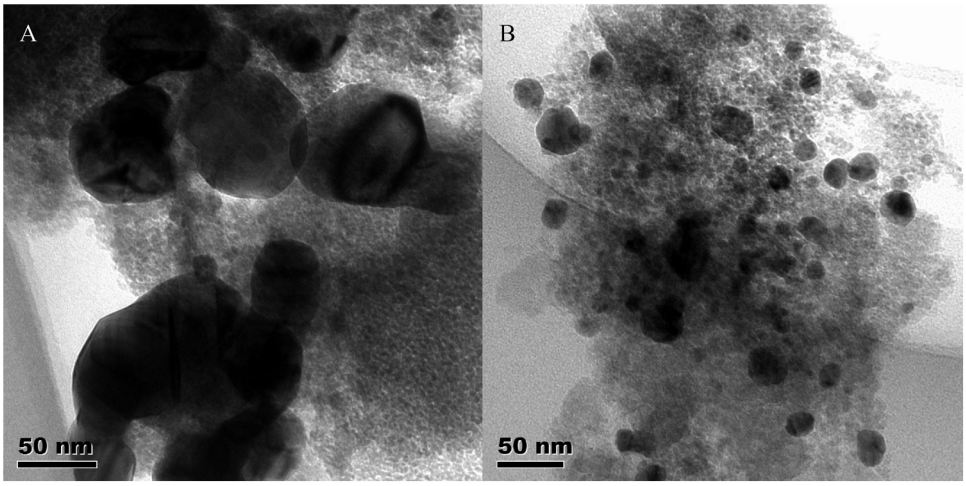

Fig. 9. TEM images of Cu_2O–Ag–AgBr/Al_2O_3: (A) after photodegradation of 2-CP under visible light irradiation (λ > 420 nm), (B) after regeneration by calcination at 500 °C.

AgBr and Cu_2O. The plasmon resonance of Ag NPs overlapped with the absorption peak of Cu_2O.

3.2. Photodegradation of pollutants under visible light irradiation

Fig. 5 showed photocatalytic degradation of 2-CP under visible light illuminated catalysts ($\lambda > 420$ nm). Only about 4.2% and 6.3% of 2-CP was adsorbed after 30 min under dark condition for Ag–AgBr/Al_2O_3 and Cu_2O–Ag–AgBr/Al_2O_3 respectively. 2-CP was completely photodegraded within 15 min in the Cu_2O–Ag–AgBr/Al_2O_3 suspension while the same results were obtained within 25 min in the Ag–AgBr/Al_2O_3 suspensions. In addition, 2,4-dichlorophenol (2,4-DCP), 2,4,6-trichlorophenol (TCP) and pentachlorophenol (PCP) were completely degraded within 21 min, 27 min and 6 min, respectively, in Cu_2O–Ag–AgBr/Al_2O_3 suspension under visible light irradiation (Fig. S1A). 68%, 45% and 56% of TOC were removed after 30 min for 2,4-DCP, TCP and PCP, respectively (Fig. S1B). These results indicated that Cu_2O–Ag–AgBr/Al_2O_3 was effective photocatalyst under visible light irradiation. The efficient charge separation and high transport of the photogenerated electrons and holes should be the crucial factor for the photocatalytic activity enhancement of Cu_2O–Ag–AgBr/Al_2O_3.

3.3. Photostability and Ag^+ releasing of Cu_2O–Ag–AgBr/Al_2O_3

The metal ions dissolution from different catalysts were examined during the photodegradation of 2-CP under visible light ($\lambda > 420$ nm). As shown in the inset of Fig. 5, the concentration of Ag^+ dissolved from Ag–AgBr/Al_2O_3 was significantly high and the initial value reached to 15.54 mg/L. The concentration of Ag^+ in solution gradually decreased with increasing reaction time, indicating that the dissolved Ag^+ was photoreduced to Ag^0 and re-deposited onto the surface of the catalyst again. In contrast, the Ag^+ release was greatly inhibited in Cu_2O–Ag–AgBr/Al_2O_3 suspension. Very low Ag^+ releasing (0.01–0.29 mg/L) appeared and no Cu^{2+} was detected throughout the entire reaction. The final concentration of Ag^+ was 0.29 mg/L in Cu_2O–Ag–AgBr/Al_2O_3, approximately six times less than the 1.74 mg/L concentration observed in the Ag–AgBr/Al_2O_3 suspension. The photocatalytic activity of Cu_2O–Ag–AgBr/Al_2O_3 markedly decreased after one cycle of degradation under visible irradiation. Only about 30% 2-CP was degraded within 30 min in used Cu_2O–Ag–AgBr/Al_2O_3 suspension. In contrast, after reactivation by washed and dried at 100 °C, and then calcinated at 500 °C for 3 h, the photoactivity of the used sample was nearly recovered. By the same reactivation procedure, Cu_2O–Ag–AgBr/Al_2O_3 exhibited excellent stability for five cycles of degradation testing under visible-light irradiation (Fig. 6).

In order to study the change of Cu_2O–Ag–AgBr/Al_2O_3 particles in the photocatalytic process, the used samples irradiated for 30 min and 40 h in 2-CP solution were characterized by XRD, XPS and TEM. As shown in Fig. 7, the diffraction peaks of Ag^0 became stronger, especially in the sample for 40 h irradiation, indicating more Ag^0 formation during the photodegradation process of 2-CP. Besides this, a new diffraction peak at 18° appeared with 40 h irradiation, which was possibly assigned to Ag_2O (JCPDS 72-2108). According the AES analysis (Fig. 8), the Auger parameters of surface Ag in the used samples irradiated for 30 min, were 725.96 eV and 724.26 eV assigned to Ag^0 and Ag^+, respectively, which demonstrated that the surface Ag species coexist as Ag^+ and Ag^0 in used samples. The results confirmed the formation of Ag^0 on the surface of catalyst during the photocatalytic reaction. Moreover, both the Cu^+ and Cu^{2+} still existed on the surface of used Cu_2O–Ag–AgBr/Al_2O_3, the atomic percentage of Cu^+ in mixture of surface Cu^+ and Cu^{2+} was 42.2%. Even for the sample irradiated for 40 h, the ratio of Cu^+ in surface Cu was still 40.4%. As shown in TEM (Fig. 9), the nanocomposite particles, after irradiation by visible light for 40 h, exhibited

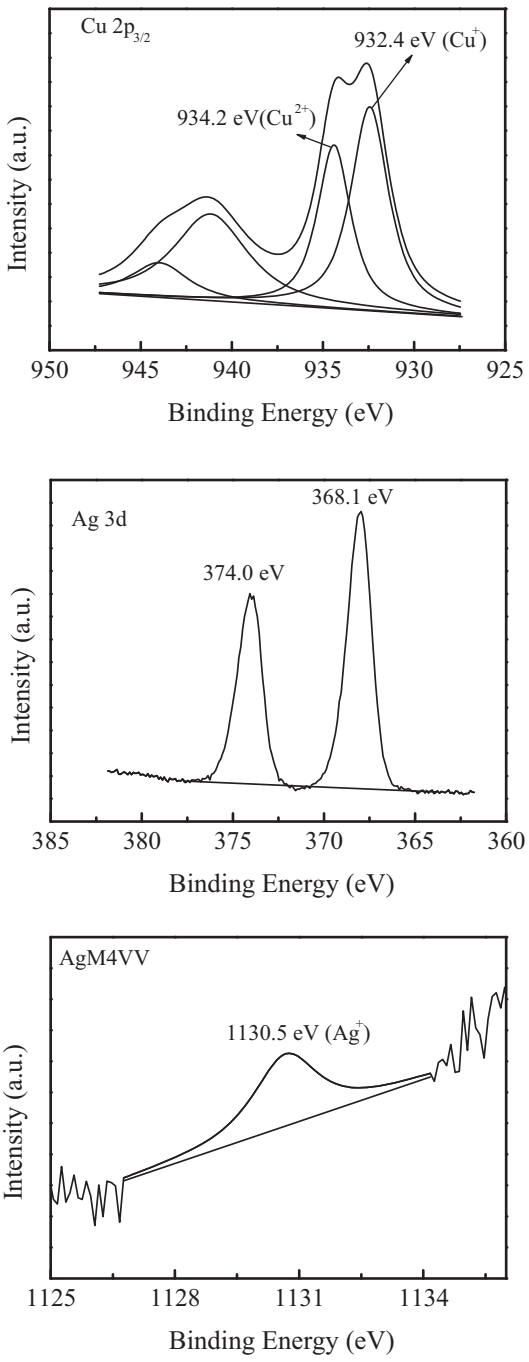

Fig. 10. Cu 2p XPS, Ag 3d XPS and Ag AES spectra for the reactivated Cu_2O–Ag–AgBr/Al_2O_3 sample after 40 h visible light irradiation.

bigger particle size in the range of 50–150 nm and lower dispersion on the surface of Al_2O_3. However, the particles became smaller again after the catalyst regeneration, and the surface Ag species existed predominantly in the Ag^+ form again by XPS and AES measurements (Fig. 10), while the atomic percentage of Cu^+ in surface state Cu did not obviously change and was about 39.6%. Therefore, the formation of bigger Ag^0 cluster leaded to the decrease of the photocatalyst activity because the surface plasmon resonance of Ag NPs depended on particle size [32–34]. In contrast, Ag–AgBr/Al_2O_3 exhibited activity successive cycles without any treatment [27], indicating no formation of the bigger Ag^0 cluster in the process of photocatalysis. The results verified that the faster transfer of electron occurred between Ag^+ and Ag^0 on the surface of

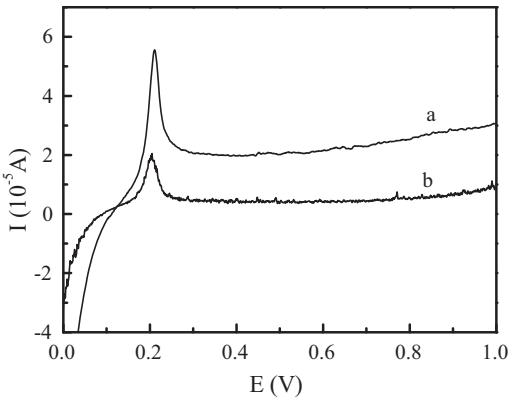

Fig. 11. The photocurrents at the different photoanode in N_2-saturated 0.1 M sodium sulfate aqueous solutions under visible light irradiation: (a) Ag–AgBr/Al_2O_3, (b) Cu_2O–Ag–AgBr/Al_2O_3.

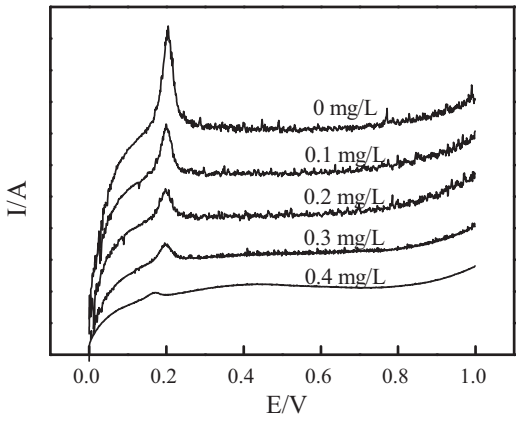

Fig. 12. The photocurrent change at the Cu_2O–Ag–AgBr/Al_2O_3 photoanode with addition of 2-CP in N_2-saturated 0.1 M Na_2SO_4 solution.

Cu_2O–Ag–AgBr/Al_2O_3 than Ag–AgBr/Al_2O_3, causing the bigger Ag^0 cluster formation. Cu_2O is the oxides with high level of conduction bands (CB), so the photogenerated electron can transfer from its CB to Ag NP, enhancing the reduction of Ag^+ induced by plasmon resonance to lead the bigger Ag^0 cluster. The result confirmed that the coupling of Cu_2O with AgBr and Ag NPs accelerated the interconversion between Ag^+ and Ag^0, then dissolved Ag^+ was re-deposited on the surface again rather than diffuse to aqueous. On the other hand, the single Cu_2O could be oxidized fully to CuO after irradiation of several hours due to the lower valence band (VB) edge level than the oxidation potential of Cu_2O to CuO [26]. However, the incorporated Cu_2O exhibited high stability, indicating the consumption of photogenerated holes in the VB of Cu_2O in Cu_2O–Ag–AgBr/Al_2O_3 suspension. Therefore, the coupling of Cu_2O with Ag NPs and AgBr in Cu_2O–Ag–AgBr/Al_2O_3 not only inhibited the releasing of Ag^+, but it also was beneficial to remain Cu_2O stable.

3.4. Interfacial charge transfer in Cu_2O–Ag–AgBr/Al_2O_3

In order to illustrate the effect of Cu_2O on the charge separation and charge-transfer processes, CV analyses were performed at the different photoanodes in a N_2-saturated 0.1 M sodium sulfate aqueous solution under $\lambda > 420$ nm visible light irradiation (Fig. 11). Under visible irradiation, the photocurrent increased and then decreased to a stable value, resulting in a peak at 0.21 V on Ag–AgBr/Al_2O_3, which was assigned to the oxidation of Ag NPs due to the plasmon-induced charge separation [14,18,27]. The peak with weaker intensity was also observed on Cu_2O–Ag–AgBr/Al_2O_3 photoanodes, indicating the lower amount Ag NPs were photocorrosioned in the presence of Cu_2O. On the other hand, a indiscernible peak at 0.63 V appeared on Cu_2O/Al_2O_3 photoanode, due to the oxidation of Cu^+ by the generated hole (Fig. S2). Conversely, the same peak did not appeared at Cu_2O–Ag/Al_2O_3 (Fig. S2) and Cu_2O–Ag–AgBr/Al_2O_3 photoanodes due to the role of Ag NPs and AgBr, respectively. Moreover, the oxidation peak of Ag NPs also did not appeared in Cu_2O–Ag/Al_2O_3 because the photogenerated electrons in Cu_2O can transfer to Ag NPs [35].

When the Cu_2O–Ag–AgBr/Al_2O_3 system was irradiated with visible light ($\lambda > 420$ nm), several electron transfers occurred at the interface of the catalyst with water. Firstly, the electrons from the plasmon-excited Ag NPs transferred to the CB of AgBr, resultant of the oxidation of Ag. The oxidation peaks of Ag NPs gradually decreased with the addition of 2-CP to act as electron donors (Fig. 12), suggesting an electron transfer from 2-CP to the Ag NPs. This result revealed that 2-CP could be oxidized by plasmon-induced h^+ on Ag NPs, confirmed that plasmon-induced h^+ on Ag NPs was an active species. Second, the electrons from photoexcited Cu_2O transferred to Ag NPs to reduce the oxidized silver. Therefore, the oxidation peak of Ag NPs at Cu_2O–Ag–AgBr/Al_2O_3 became weaker than Ag–AgBr/Al_2O_3. In addition, the CB level of Cu_2O lies at −1.4 eV [24], which is more negative than the CB level of AgBr (−1.04 eV, NHE) [36]. Therefore, the photogenerated electron in the CB of Cu_2O particles could also transfer to the AgBr and are further trapped by O_2 to form $O_2^{\bullet -}$, whereas photo-generated holes in VB of AgBr particles migrate the surface of Cu_2O particles.

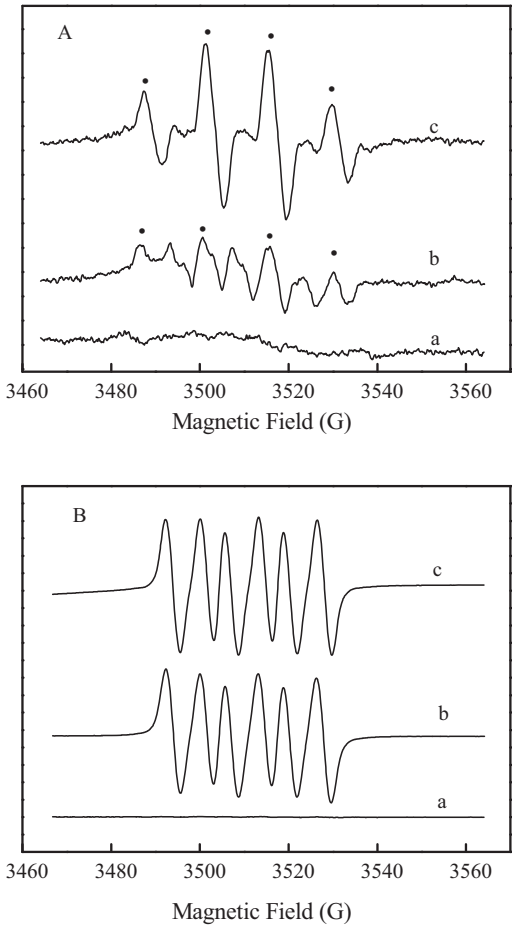

Fig. 13. BMPO spin-trapping ESR spectra recorded at ambient temperature in aqueous dispersion (for BMPO-•OH, A) and methanol dispersion (for BMPO-$O_2^{\bullet -}$, B): (a) BMPO control, (b) Ag–AgBr/Al_2O_3, (c) Cu_2O–Ag–AgBr/Al_2O_3 with $\lambda > 420$ nm visible light irradiation.

Furthermore, the deduction was confirmed by the ESR studies. As shown in Fig. 13, the almost same amount of $O_2^{\bullet-}$ was generated in Cu_2O–Ag–AgBr/Al_2O_3 and Ag–AgBr/Al_2O_3 suspensions under visible light irradiation. However, more $^{\bullet}OH$ was formed in Cu_2O–Ag–AgBr/Al_2O_3 suspensions than that in Ag–AgBr/Al_2O_3 under otherwise conditions. The results clearly indicated that holes accumulated in the VB of Cu_2O were also available for the formation of $^{\bullet}OH$. Previous study already confirmed that although the oxidation of water by holes at Cu_2O is thermodynamically possible due to the redox potential of holes in the VB of Cu_2O (1.92 V vs. NHE) being more positive than that of the couple H_2O/O_2 (1.23 V vs. NHE), the reaction is kinetically sluggish [35]. As a result, the oxidation of water at Cu_2O was neglected in this pathway. Similarly, in our experiment, neither $^{\bullet}OH$ signal was detected in Cu_2O/Al_2O_3 (the date was not shown here). Therefore, the stronger $^{\bullet}OH$ signal indicated that the co-existence of AgBr and Ag facilitated the oxidation of water to $^{\bullet}OH$ by the holes in the VB of Cu_2O, and the photocorrosion of Cu_2O was inhibited as well. On the basis of all the information, the presence of Cu_2O in the Cu_2O–Ag–AgBr/Al_2O_3 accelerated the plasmon-induced charge separation and transfer process, not only improved the activity of degradation of pollutants, but also suppressing the Ag^+ releasing to water. In turn, the photocorrosion of Cu_2O was restrained to some extent due to the co-existence of Ag and AgBr.

4. Conclusions

Cu_2O–Ag–AgBr nanocomposite was deposited onto Al_2O_3 by a deposition–precipitation method. The catalyst showed high photocatalytic activity for the degradation of organic pollutants under visible light irradiation. Furthermore, the release of metal ions from the catalyst was significantly inhibited. CV analyses and the formation of Ag^0 cluster on the surface during the photodegradation of pollutants verified four electron-transfer processes occurred during the degradation of 2-CP: (I) electron transfer occurred from the plasmon-photoexcited Ag NPs to the CB of AgBr, resulting in the formation of $O_2^{\bullet-}$; (II) electron from the CB of Cu_2O to the Ag NPs and (III) electron transfer from 2-CP to the Ag NPs, accelerating the photoxized Ag NPs back to their initial state, suppressing Ag^+ dissolution; (IV) electron form the CB of Cu_2O to the CB of AgBr, improving the charge separation rate.

Acknowledgments

This work was supported by the NSFC (Nos. 21125731 and 51221892) and the Project 973 (No. 2010CB933604).

Appendix A. Supplementary data

Supplementary data associated with this article can be found, in the online version, at http://dx.doi.org/10.1016/j.apcatb.2014.02.003.

References

[1] J. Cao, B. Luo, H. Lin, B. Xu, S. Chen, Journal of Hazardous Materials 217–218 (2012) 107–115.
[2] V. Subramanian, E.E. Wolf, P.V. Kamat, Journal of the American Chemical Society 126 (2004) 4943–4950.
[3] K. Awazu, M. Fujimaki, C. Rockstuhl, J. Tominaga, H. Murakami, Y. Ohki, N. Yoshida, T. Watanabe, Journal of the American Chemical Society 130 (2008) 1676–1680.
[4] M. Valden, X. Lai, D.W. Goodman, Science 281 (1998) 1647–1650.
[5] P. Andrew, W.L. Barnes, Science 306 (2004) 1002–1005.
[6] S. Linic, P. Christopher, D.B. Ingram, Nature Materials 10 (2011) 911–921.
[7] D.B. Ingram, S. Linic, Journal of the American Chemical Society 133 (2011) 5202–5205.
[8] J.-J. Chen, J.C.S. Wu, P.C. Wu, D.P. Tsai, Journal of Physical Chemistry C 116 (2012) 26535–26542.
[9] S. Wang, B. Zhang, Applied Catalysis B: Environmental 467 (2013) 585–592.
[10] D. Zhang, M. Wen, S. Zhang, P. Liu, W. Zhu, G. Li, H. Li, Applied Catalysis B: Environmental 147 (2014) 610–616.
[11] X. Bai, R. Zong, C. Li, D. Liu, Y. Liu, Y. Zhu, Applied Catalysis B: Environmental 147 (2014) 82–91.
[12] P. Christopher, H. Xin, S. Linic, Nature Chemistry 3 (2011) 467–472.
[13] L.-W. Zhang, Y.-J. Wang, H.-Y. Cheng, W.-Q. Yao, Y.-F. Zhu, Advanced Materials 21 (2009) 1286–1290.
[14] C. Hu, T. Peng, X. Hu, Y. Nie, X. Zhou, J. Qu, H. He, Journal of the American Chemical Society 132 (2010) 857–862.
[15] H. Zhang, X. Fan, X. Quan, S. Chen, H. Yu, Environmental Science and Technology 45 (2011) 5731–5736.
[16] Y. Tian, T. Tatsuma, Journal of the American Chemical Society 127 (2005) 7632–7637.
[17] S.K. Cushing, J. Li, F. Meng, T.R. Senty, S. Suri, M. Zhi, M. Li, A.D. Bristow, N. Wu, Journal of the American Chemical Society 134 (2012) 15033–15041.
[18] X. Zhou, C. Hu, X. Hu, T. Peng, Journal of Hazardous Materials 219–220 (2012) 276–282.
[19] E. Kazuma, T. Tatsuma, Chemical Communications (2012) 1733–1735.
[20] S.C. Warren, E. Thimsen, Energy and Environmental Science 5 (2012) 5133–5146.
[21] V. Subramanian, E.E. Wolf, P.V. Kamat, Langmuir 19 (2003) 469–474.
[22] T. Peng, C. Hu, X. Hu, X. Zhou, J. Qu, Catalysis Letters 142 (2012) 646–654.
[23] A.M. Kalsin, M. Fialkowski, M. Paszewski, S.K. Smoukov, K.J.M. Bishop, B.A. Grzybowski, Science 312 (2006) 420–424.
[24] L. Xiong, M. Ouyang, L. Yan, J. Li, M. Qiu, Y. Yu, Chemistry Letters 38 (2009) 1154–1155.
[25] Y. Bessekhouad, D. Robert, J.V. Weber, Catalysis Today 101 (2005) 315–321.
[26] L. Huang, F. Peng, H. Yu, H. Wang, Solid State Sciences 11 (2009) 129–138.
[27] X. Zhou, C. Hu, X. Hu, T. Peng, J. Qu, Journal of Physical Chemistry C 114 (2010) 2746–2750.
[28] B. Xu, T. Xiao, Z. Yan, X. Sun, J. Sloan, S.L. González-Cortésa, F. Alshahrani, M.L.H. Green, Microporous and Mesoporous Materials 91 (2006) 293–295.
[29] L. Gou, C.J. Murphy, Nano Letters 3 (2003) 231–234.
[30] S.G. Aspromonte, R.M. Serra, E.E. Miró, A.V. Boix, Applied Catalysis A: General 407 (2011) 134–144.
[31] C. Hu, Y. Lan, J. Qu, X. Hu, A. Wang, Journal of Physical Chemistry B 110 (2006) 4066–4072.
[32] P.V. Kamat, Journal of Physical Chemistry B 106 (2002) 7729–7744.
[33] H. Xu, H. Li, J. Xia, S. Yin, Z. Luo, L. Liu, L. Xu, ACS Applied Materials and Interfaces 3 (2011) 22–29.
[34] C. Tabor, R. Murali, M. Mahmoud, M.A. El-Sayed, Journal of Physical Chemistry A 113 (2008) 1946–1953.
[35] S. Wei, J. Shi, H. Ren, J. Li, Z. Shao, Journal of Molecular Catalysis A: Chemical 378 (2013) 109–114.
[36] M. Asi, C. He, M. Su, D. Xia, L. Lin, H. Deng, Y. Xiong, R. Qiu, X. Li, Catalysis Today 175 (2011) 256–263.